

## Where are the Baryons?

Renyue Cen<sup>1</sup> and Jeremiah P. Ostriker<sup>2</sup>

Received \_\_\_\_\_; accepted \_\_\_\_\_

---

<sup>1</sup>Princeton University Observatory, Princeton University, Princeton, NJ 08544;  
cen@astro.princeton.edu

<sup>2</sup>Princeton University Observatory, Princeton University, Princeton, NJ 08544;  
jpo@astro.princeton.edu

## ABSTRACT

New, high resolution, large-scale, cosmological hydrodynamic galaxy formation simulations of a standard cold dark matter model (with a cosmological constant) are utilized to predict the distribution of baryons at the present and at moderate redshift. It is found that the average temperature of baryons is an increasing function of time, with most of the baryons at the present time having a temperature in the range  $10^{5-7}$  K. Thus, not only is the universe dominated by dark matter, but more than one half of the normal matter is yet to be detected. Detection of this warm/hot gas poses an observational challenge, requiring sensitive EUV and X-ray satellites. Signatures include a soft, cosmic X-ray background, apparent warm components in hot clusters due to both intrinsic warm intra-cluster gas and warm inter-cluster gas projected onto clusters along the line of sight, absorption lines in X-ray and UV quasar spectra [e.g., O VI (1032,1038)A lines, OVII 574 eV line], strong emission lines (e.g., O VIII 653 eV line) and low redshift, broad, low column density Ly $\alpha$  absorption lines. We estimate that approximately 1/4 of the extragalactic soft X-ray background (SXRB) (at 0.7 keV) arises from the warm/hot gas, half of it coming from  $z < 0.65$  and three-quarters from  $z < 1.00$ , so the source regions should be identifiable on deep optical images.

*Subject headings:* Cosmology: large-scale structure of Universe – cosmology: theory – galaxies: clustering – galaxies: formation – numerical method

## 1. Introduction

Where are the baryons, the ordinary non-exotic matter of the universe? If we consider the universe at redshift two, a consistent picture emerges: the amount of mass seen directly by the Hubble Space Telescope (HST) in stellar systems is very small ( $\Omega_* \approx 5.5 \times 10^{-4}$  [for  $h=0.70$ ]; Madau, Pozzetti, & Dickinson 1998), when compared either to the amount seen in the local universe or to the critical cosmological density. But the amount of hydrogen and helium observed as absorption lines in the Lyman alpha forest is considerable. Recent analyses (Rauch et al. 1997; Weinberg et al. 1997) give

$$\Omega_{baryon} \geq 0.017h^{-2} = 0.035 \quad (1)$$

from observations of the Lyman alpha forest at redshift two, where  $\Omega_{baryon}$  is the density in units of the critical density,  $h \equiv H/100\text{km/s/Mpc}$ , and  $h = 0.70$  is adopted for the last term in equation (1). It is worth noting that the above quoted lower limit on  $\Omega_{baryon}$  might be too conservative by as much as a factor of  $\sim 2 - 7$ , due primarily to the uncertainty in the observationally determined metagalactic radiation field.

The observed light-element ratios, combined with standard nucleosynthesis, allow to compute the expected baryon density for standard models (Burles & Tytler 1998) as

$$\Omega_{baryon} = (0.019 \pm 0.001)h^{-2} = 0.039 \pm 0.002. \quad (2)$$

The approximate consistency between these two completely independent methods of estimating the baryon density is reassuring, as is the fact that theoretical models incorporating (1), (2) and standard theory for the growth of structure reproduce, in great detail, numerous features (column density dependence, redshift dependence, spatial correlations, etc) of the observed Lyman alpha forests (Cen et al. 1994; Zhang et al. 1995; Miralda-Escudé et al. 1995; Hernquist et al. 1996).

But at redshift zero, in the present day universe, every analysis (e.g., Fukugita, Hogan,

& Peebles 1997) indicates that, after summing over all well observed contributions, the local baryon density appears to be far lower than indicated by equation (1) and (2):

$$\Omega_* + \Omega_{HI} + \Omega_{H_2} + \Omega_{X_{ray,cl}} \approx 0.0068 \leq 0.011 \quad (2\sigma \text{ limit}) \quad (3)$$

for  $h = 0.70$ . Thus, either most of the baryons in the present day universe are yet to be detected or a serious error has been made in the arguments that led to equations (1) and (2). Several authors (e.g., Wolfe et al. 1995) have noticed that the mass density seen in the damped Lyman alpha systems at moderate redshift ( $z \sim 3$ ) approximately corresponds to the mass density in the stellar component of galaxies at  $z = 0$ . While important and roughly true, this point does not help us much, since only a small fraction (approximately 4%) of the Lyman alpha forest is seen in the neutral high column density damped systems and, correspondingly,  $\Omega_*$  is about 0.003.

Thus, the puzzling question remains. Where are the baryons in the universe today? There have been a number of proposals to account for the missing baryons (O’Neil 1997; Burkert & Silk 1997; Bristow & Phillips 1994). Now, the whereabouts and state of those missing baryons can be computed from standard initial conditions, in realistic large-scale cosmological hydrodynamic simulations. We have concluded that a substantial fraction of the missing baryons are to be found in intergalactic gas in a temperature range  $10^5 < T < 10^7 \text{ K}$ , where they have been difficult to detect and which we call “warm/hot gas”. The paper is organized as follows. A brief descriptions of the simulations is presented in §2. Results are given in §3 and §4 concludes the paper with a discussion of the robustness of the results and ways to detect this warm/hot gas.

## 2. Simulation

This result is based on a computation of the evolution of the gas in a cold dark matter model with a cosmological constant; the model is normalized to both the microwave background temperature fluctuations measured by COBE on large scales (Bunn & White 1997) and the observed abundance of clusters of galaxies in the local universe (e.g., Cen 1998), and it is close to both the concordance model of Ostriker & Steinhardt (1995) and the model indicated by the recent high redshift supernova results (Riess et al. 1997). The relevant model parameters are:  $\Omega_0 = 0.37$ ,  $\Omega_{baryon} = 0.049$ ,  $\Lambda_0 = 0.63$ ,  $\sigma_8 = 0.80$ ,  $h = 0.70$ ,  $n = 0.95$  and 25% tensor mode contribution to the CMB fluctuations on large scales. Two simulations with box sizes of  $L_{box} = (100, 50)h^{-1}\text{Mpc}$  are made, each having  $512^3$  cells and  $256^3$  dark matter particles. The conclusions drawn in this paper are not significantly affected by the finite resolution. Although based on simulations of a specific model, we believe that the result is generic and would occur in any model consistent with other large scale structure results. The description of the numerical methods of the cosmological hydrodynamic code and input physical ingredients will be presented elsewhere. To briefly recapitulate, we follow three components separately and simultaneously: dark matter, gas and galaxies, where the last component is created continuously from the former two during the simulations in places where real galaxies are thought to form as dictated mostly by local physical conditions. Self-consistently, feedback into the intergalactic medium (IGM) from young stars in the “galaxies” is allowed, in three related forms: supernova thermal energy output, UV photon output and mass ejection from the supernova explosions. The model reproduces the observed UV background and metallicity distributions among others.

### 3. Results

Before describing our detailed results, it is useful to give a simple and surprisingly accurate order of magnitude physical argument. In all standard pictures for the growth of structure there is imprinted at an early time a spectrum of perturbations, with the amplitude of the fluctuations being largest at small scales and smaller at larger scales. After decoupling at  $z \sim 1000$ , all waves grow (due to self-gravity) roughly as  $(1+z)^{-1}$ . They have reached the nonlinear length and mass scales of  $5.6h^{-1}\text{Mpc}$  and  $7.5 \times 10^{13}h^{-1}\text{M}_\odot$ , respectively, by  $z = 0$  (our fiducial model is adopted for this illustration). When a perturbation of a given scale  $L$  collapses at time  $t$  due to gravity, geometry indicates it must do so with a velocity  $v \approx L/t$  and, as opposite sides of the collapsing perturbation meet and attempt to cross one another, a shock is generated behind which the sound speed is  $C \approx v$ . Combining these simple arguments and noting that  $t^{-1} \approx H$  gives us

$$C_z^2 = K(HL_{nl})_z^2, \quad (4)$$

where  $K$  is a numerical constant and  $H_z$  and  $L_{nl,z}$  are the Hubble constant and nonlinear length scale at epoch  $z$ , respectively. Applying this to the current epoch (with  $K = 1$ ) gives  $C_o = 565\text{km/s}$ , which corresponds to a temperature of  $3.9 \times 10^7\text{K}$ . This should correspond to the typical temperature of recently collapsed (i.e. high density) objects, with the global mean temperature somewhat lower. Note that  $K$  is only a dimensionless number to indicate the nature of the scaling relation and is not intended to model shock jump conditions.

Figure 1 shows the mean computed temperature as a function of redshift from the  $[100h^{-1}\text{Mpc}]^3$  simulation. The volume weighted average temperature at  $z = 0$  is  $10^{5.5}\text{K}$ , the mass ( $\rho$ ) weighted average temperature is  $10^{7.4}\text{K}$  (the value given by equation 1 with  $K = 1$ ) and the  $\rho^2$  weighted average (roughly speaking emission weighted) is  $10^{8.0}\text{K}$ . Thus, the high density regions are in just the temperature domain indicated by equation (4) with the constant taken to be unity. Figure 1 shows that equation (4) (adopting  $K = 1$ ) in fact

roughly tracks the density weighted averages from redshift three onwards, confirming the simple physical picture presented earlier.

Now let us examine the results in greater detail, dividing the gas into three temperature ranges (1)  $T > 10^7$  K (the normal X-ray emitting gas, predominantly in collapsed and virialized clusters of galaxies); (2)  $10^7 \text{ K} > T > 10^5 \text{ K}$  gas, which we will call the warm/hot gas and is mainly in unvirialized regions; (3)  $T < 10^5 \text{ K}$  warm gas, which is seen in optical studies both in absorption and emission. A last component (4) is the cold gas that has been condensed into stellar objects, which we designate “galaxies”, and which will contain stars and cold gas. Figure 2 shows the evolution of these four components, and the results are consistent with our other knowledge. Most of the volume is always filled with warm (Lyman alpha forest) gas, but the mass fraction in this component declines from 94% at  $z = 3$  to 26% at  $z = 0$ , consistent with the HST observed clearing of the forest and of low- $z$  redshift Ly $\alpha$  cloud gas (Shull 1996, 1997). Note that at low redshift denser gas in and around galaxy halos may make significant contributions to the observed low redshift Ly $\alpha$  clouds, which compensates somewhat the decrease of the warm component and incidentally leads to a leveloff of Ly $\alpha$  clouds at low redshift (Bahcall et al. 1996). The hot component increases in mass fraction, reaching 12% by mass at  $z = 0$ , and is consistent with observations of the local properties of the X-ray emitting great clusters (e.g., Cen & Ostriker 1994; Bryan & Norman 1998). The condensed component remains small (12% and is possibly overestimated in this simulation), consistent with the known mass density in galaxies.

But we wish to focus attention on the solid circles in Figure 2b: the warm/hot gas rises dramatically in abundance with increasing time and dominates the mass balance by  $z = 0$ , reaching 52% of the noncondensed mass fraction or 47% of the total baryons.

Figure 3 shows the spatial distribution of this gas. We see a filamentary structure (in green) where, at the high density nodes (red), “galaxies” have formed or been collected.

The spectral features of this warm/hot gas are in the EUV and soft X-ray, which are very difficult to observe at low redshift because of the interstellar medium in the Galaxy. In the soft X-ray the Galaxy is a strong source of emission at an effective temperature of  $\sim 10^6$ K, whereas the neutral hydrogen in the Galaxy prevent observations of the EUV at  $\lambda < 912\text{\AA}$ .

Finally, Figure 4 shows the distribution of emission of the gas, which convolves the density weighted distribution with the familiar cooling curve  $\Lambda(T)$ . We see, at  $z = 0$ , two peaks, one at  $10^8$ K and a higher and broader one at  $10^5$ K, with a broad flat valley in between. Note that cooling due to metals is included in the calculation, where metals are produced self-consistently in the simulation. The computed metallicities are consistent with observations where comparisons can be made.

#### 4. Discussion

How robust are these results to variation of model assumptions? We believe that any model which is consistent with other well measured local universe observations would give essentially the same result. The reason for this is simply that the temperature is determined by the nonlinear mass scale (equation 4), and that, in turn is close to the  $8h^{-1}\text{Mpc}$  scale which fixes the abundance of rich clusters and is fairly robustly determined to a narrow range (e.g., Cen 1998):  $\sigma_8 \approx (0.50 \pm 0.05)\Omega_0^{-0.40}$  for  $0.2 < \Omega_0 < 1.0$ . Only a very small extrapolation is needed to go from this well observed scale to the nonlinear scale, so the estimated temperature of collapsed regions that we find will be common to all models based on the gravitational growth of structure - as normalized to local cluster observations. In fact, analysis of our earlier work (Ostriker & Cen 1995) covering nearly a dozen different models (at lower resolution) has shown that from one-half to two-thirds of all baryons in all models are consistently and robustly in this warm/hot gas at  $z = 0$ . We also show in Figure 2b the warm/hot component for two other models, an open CDM model with  $\Omega_0 = 0.40$  and

$\sigma_8 = 0.75$  (dotted curves), and a mixed hot and cold dark matter model with  $\Omega_{hot} = 0.30$  and  $\sigma_8 = 0.67$  (dashed curves) computed completely independently by Bryan & Norman (1998). Yet, their results are in excellent agreement with ours. The density fluctuation amplitude normalization of their mixed dark matter model is somewhat below that required to produce the abundance of local galaxy clusters. Therefore, an appropriately normalized mixed dark matter model would yield the warm/hot gas fraction in still better agreement with the other two models.

How robust are these results to the input modeling physics? In addition to gravity and hydrodynamics, there are three major pieces of relevant input physics: the meta-galactic radiation field, energy deposition into IGM from young galaxies and metal cooling. All these three pieces of physics are already included in the simulations examined here. Let us discuss them in turn. First, changing the meta-galactic radiation field would not make any significant difference to the baryons at the relevant temperature and density ranges, because the warm/hot gas is heated primarily by collisions. Second, energy feedback from young galaxies is secondary compared to shock heating due to structure collapse. An estimate can be made: the equivalent kinetic energy input per unit mass due to supernova energy feedback, averaged over all baryons, is  $f_{gal}e_{SN}c^2 \sim (0.1) \times (1.0 \times 10^{-5}) \times c^2 = 300^2(\text{km/s})^2$ , or  $2 \times 10^6\text{K}$ , [where  $f_{gal} \sim 0.1$  is the mass fraction of baryons that is formed into galaxies by  $z = 0$  (open squares in Figure 2b), and  $e_{SN}$  is the fraction of energy that supernovae deposit into IGM in terms of total rest mass], which is compared to the mass-weighted temperature at  $z=0$ ,  $\sim 2 \times 10^7\text{K}$  (dotted curve in Figure 1). Thus, it seems that supernova feedback contributes about 10% in the overall energy budget. Finally, the metal cooling time is  $t_{cool} = kT/n\Lambda = 4.0 \times 10^{-5}T_5/\delta\Lambda$ , where  $T_5 = T/10^5$ ,  $\delta$  is the density of the gas in units of the global baryonic mean and  $\Lambda$  is the cooling rate (Bohringer & Hensler 1989). Assuming a typical metallicity of 0.1 solar, we obtain  $t_{cool} = (1.2, 54.0, 675.0)t_H/\delta$ , at  $T = (10^5, 10^6, 10^7)\text{K}$ , respectively, where  $t_H$  is the current Hubble time. For most of

the warm/hot gas,  $\delta$  is about a few. Therefore, most of the warm/hot gas has not cooled significantly and will not be able to cool in the next Hubble time, especially considering the steady input of gravitational energy. A small fraction of gas at the lower end of the temperature range ( $T < 10^5$ ) has, of course, cooled to form galaxies and a smaller fraction will continue to cool to form more galaxies in the next Hubble time. But most of the gas, including part of the gas that may otherwise be able to cool, will likely be incorporated into larger and hotter systems, due to merger as well as breaking of still longer waves.

How can this gas be observed? Cen et al. (1995) argued, from a less accurate computation than the present one, that a significant fraction of the soft X-ray background  $< 1.0$  keV was due to this warm/hot gas and that this could be verified by association of this soft X-ray background radiation field with relatively nearby large scale structure features, as well as by the soft X-ray angular auto-correlation function (Soltan et al. 1996). A more accurate prediction is now underway. Recent ROSAT observations of the soft X-ray background (Wang & McCray 1993) seem to hint the existence of this warm/hot gas. Another useful method of detecting the soft X-ray background is to search for shadows cast by nearby neutral hydrogen-rich galaxies (Wang & Ye 1996; Barber, Roberts, & Warwick 1996) using AXAF. Second, Hellsten et al. (1998), on the basis of simulations similar to those reported on here, have predicted the existence of an X-ray absorption forest due to ionized oxygen (O VII 574 eV line) in the warm/hot temperature range. Perna & Loeb (1998) have also made similar calculations based on simplified models for the IGM. Work underway with T. Tripp and E. Jenkins indicates that vacuum UV absorption lines (OVI 1032A,1038A doublets) should be detectable by current instruments due to gas in this temperature range primarily in the distant outskirts of galaxies. Third, strong soft X-ray emission lines from highly ionized species (such as O VIII 653 eV line) should also be observable (Jahoda et al. 1998, in preparation). Fourth, recent work on EUV observations (Mittaz, Lieu, & Lockman 1998) may indicate emission structures coincident

with or projected onto rich X-ray clusters due to the warm/hot component as seen Figure 3. Fifth, the warm/hot gas may show up as very broad, relatively weak (mostly having  $N_{HI} \leq 10^{13} \text{ cm}^{-2}$  with a small fraction at higher column densities), low redshift Ly $\alpha$  clouds but observations more sensitive than current ones (Shull 1996, 1997) are required. Finally, this gas may be detected through cross-correlating soft X-ray background (Refregier, Helfand, & McMahon 1997) or Sunyaev-Zel'dovich effect (Refregier, Spergel, & Herbig 1998) with galaxies.

Overall, on the basis of preliminary computations (by scaling  $\Omega_{baryon}$  down from 0.049 to 0.037 using latest observations and noting the  $J \propto \Omega_{baryon}^2$  scaling relation), we expect that 1/4 of the extragalactic soft X-ray background (at 0.7 keV) comes from this diffuse warm/hot gas:  $J_{WH} = 7 \text{ keV/sec/cm}^2/\text{keV/sr}$  is compared to the Wang-Ye (1996) estimate of  $\geq 4 \text{ keV/sec/cm}^2/\text{keV/sr}$  for the diffuse extragalactic SXRB. Half is emitted by structures at redshift  $z < 0.65$  and three-quarters from  $z < 1.00$ ; so one should be able to identify the optical features associated with the emitting gas. In sum, several experiments using existing or planned facilities have the possibility of detecting, in a relatively precise way, the abundance and cosmic distribution of this warm/hot gaseous component of the universe, which is likely to contain most of the baryonic matter at the current epoch.

We thank Richard Mushotzky, Jim Peebles and David Spergel for useful discussions, and Greg Bryan for allowing us to show his unpublished results.

## REFERENCES

- Bahcall, J.N., et al. 1996, *ApJ*, 457, 19
- Barber, C.R., Roberts, T.P., & Warwick, R.S. 1996, *MNRAS*, 282, 157
- Bohringer, H., & Hensler, G. 1989, *A& A*, 215, 147
- Bristow, P.D., & Phillips, S. 1994, *MNRAS*, 267, 13
- Bryan, G.L., & Norman, M.L. 1998, *ApJ*, 495, 80
- Bunn, E.F., & White, M. 1997, *ApJ*, 480, 6
- Burkert, A., & Silk, J. 1997, *BAAS*, 191, 2405
- Burles, S., & Tytler, D. 1998, *ApJ*, 499, 699
- Cen, R. 1998, *ApJ*, in press
- Cen, R., Kang, H., Ostriker, J.P., & Ryu, D. 1995, *ApJ*, 451, 436
- Cen, R., Miralda-Escudé, J., Ostriker, J. P., & Rauch, M. 1994, *ApJ*, 437, L9
- Cen, R., & Ostriker, J. P., 1994, *ApJ*, 429, 4
- Fukugita, M., Hogan, C.J., & Peebles, P.J.E. 1997, preprint, astro-ph/9712020
- Hellsten, U., Gnedin, N.Y., & Miralda-Escudé, J. 1998, preprint, astro-ph/9804038
- Madau, P., Pozzetti, L., & Dickinson, M. 1998, *ApJ*, 498, 106
- Miralda-Escudé, J., Cen, R., Ostriker, J. P., & Rauch, M. 1996, *ApJ*, 471, 582
- Mittaz, J.P.D., Lieu, R., & Lockman, F.J. 1998, *ApJ*, 498, 17
- O’Neil, K. 1997, *PASP*, 109, 1395

- Ostriker, J.P., & Steinhardt, P. 1995, *Nature*, 377, 600
- Perna, R., & Loeb, A. 1998, *ApJ*, 503, L103
- Rauch, M., Miralda-Escudé, J., Sargent, W.L.W., Barlow, T. A., Weinberg, D.H., Hernquist, L., Katz, N., Cen, R., Ostriker, J.P., 1998, *ApJ*, 489, 1
- Refregier, A., Helfand, D., McMahon, R.G. 1997, *ApJ*, 479, L93
- Refregier, A., Spergel, D.N., & Herbig, T. 1998, preprint, astro-ph/9806349
- Soltan, A.M., Hasinger, G., Egger, R., Snowden, S., & Truemper, J. 1996, *A& A*, 305, 17
- Shull, J.M. 1996, *AJ*, 111, 72
- Shull, J.M. 1997, in "structure and evolution of the IGM from QSO absorption lines", ed. P. Petitjean & S. Charlot
- Wang, Q.D., & McCray, R. 1993, *ApJ*, 409, L37
- Wang, Q.D., & Ye, T. 1996, *New Astron.*, 1, 245
- Weinberg, D.H., Miralda-Escudé, J., Hernquist, L., Katz, N. 1997, *ApJ*, 490, 564
- Wolfe, A.M., Lanzetta, K.M., Foltz, C.B., & Chaffee, F.H. 1995, *ApJ*, 454, 698

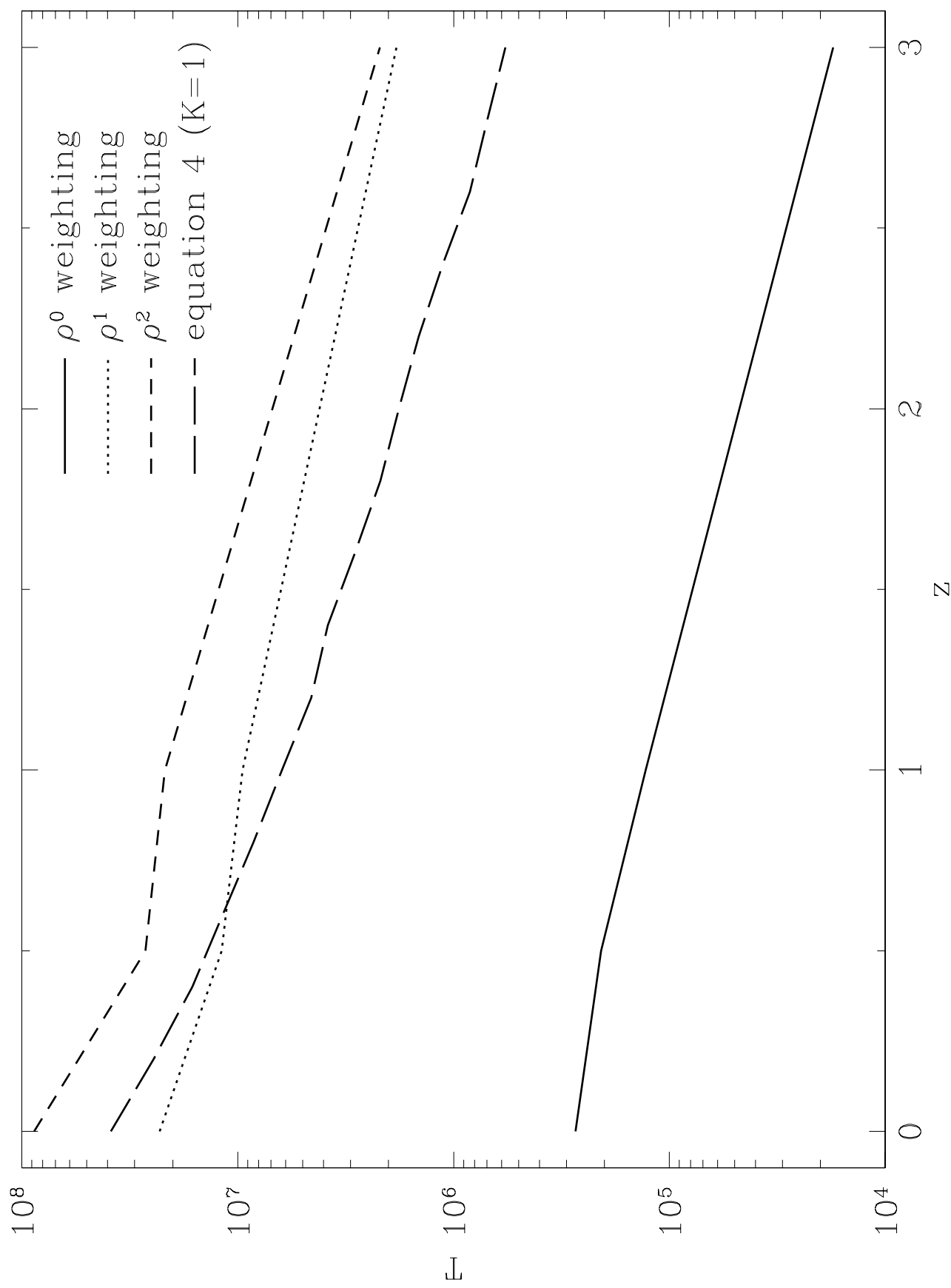
Fig. 1.— shows globally averaged temperatures within our  $[100h^{-1}Mpc]^3$  box as a function of redshift from the simulation. The solid, dotted and short-dashed curves are the average temperatures weighted by volume, density and density squared, respectively. The long-dashed curve represents the results from the simple physical argument as indicated by equation 4 with the constant  $K = 1$ , and indicates that the temperature of the high density nonlinear regions is well represented by that formula.

Fig. 2.— shows the evolution of the four components of cosmic baryons (see text for definitions). Panel (a) shows the volume fractions of the four components and panel (b) shows the mass fractions. Examination of (2b) shows that more than half of the baryons at redshift zero are in the temperature range  $10^7\text{K} > T > 10^5\text{K}$ . Also shown are the warm/hot component for two other models: an open CDM model with  $\Omega_0 = 0.40$  and  $\sigma_8 = 0.75$  (dotted curves), and a mixed hot and cold dark matter model with  $\Omega_{hot} = 0.30$  and  $\sigma_8 = 0.67$  (dashed curves). These two models were computed completely independently by Bryan & Norman (1998).

Fig. 3.— shows the spatial distribution of the warm/hot gas with temperature in the range  $10^{5-7}\text{K}$  at  $z = 0$ . The green regions have densities about ten times the mean baryon density of the universe at  $z = 0$ ; the yellow regions have densities about one hundred times the mean baryon density, while the small isolated regions with red and saturated dark colors have even higher densities reaching about a thousand times the mean baryon density, and are sites for current galaxy formation.

Fig. 4.— shows the distribution of emission of the gas which convolves the density weighted distribution with the familiar cooling curve  $\Lambda(T)$ , including emission from metals where are computed self-consistently in the simulation. Three epochs,  $z = (0, 1, 3)$ , are shown as solid, dotted and dashed curves, respectively. At redshift zero most of the emission is from the warm/hot gas with a secondary maximum at the normal hard X-ray peak of  $10^8\text{K}$ .

Figure 1



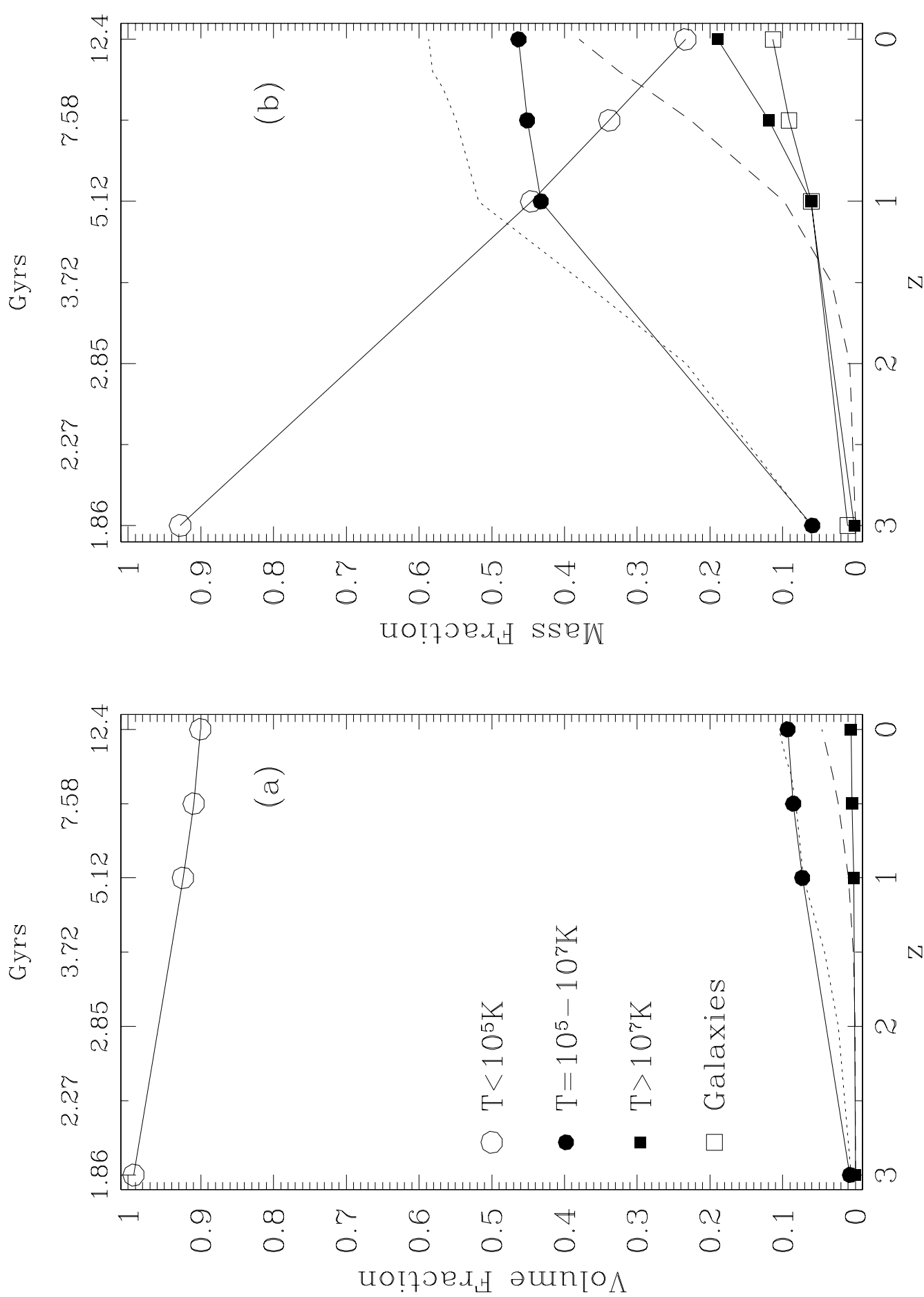


Figure 2

This figure "fig3\_warm.jpg" is available in "jpg" format from:

<http://arxiv.org/ps/astro-ph/9806281v4>

Figure 4

